ARTICLES
PUBLISHED ONLINE: 29 SEPTEMBER 2013 | DOI: 10.1038/NPHOTON.2013.247
nature photonics

Trapping light by mimicking gravitational lensing

C. Sheng[1], H. Liu[1]*, Y. Wang[1], S. N. Zhu[1] and D. A. Genov[2]

One of the most fascinating predictions of the theory of general relativity is the effect of gravitational lensing, the bending of light in close proximity to massive stellar objects. Recently, artificial optical materials have been proposed to study the various aspects of curved spacetimes, including light trapping and Hawking radiation. However, the development of experimental 'toy' models that simulate gravitational lensing in curved spacetimes remains a challenge, especially for visible light. Here, by utilizing a microstructured optical waveguide around a microsphere, we propose to mimic curved spacetimes caused by gravity, with high precision. We experimentally demonstrate both far-field gravitational lensing effects and the critical phenomenon in close proximity to the photon sphere of astrophysical objects under hydrostatic equilibrium. The proposed microstructured waveguide can be used as an omnidirectional absorber, with potential light harvesting and microcavity applications.

During the total solar eclipse in 1919, Arthur Eddington and collaborators performed the first direct observation of light deflection from the Sun, thereby validating Einstein's theory of general relativity[1]. According to Einstein's theory, the presence of matter energy results in curved spacetime and the complex motion of matter and light along geodesic trajectories that are no longer straight lines. The general theory of relativity has been highly successful, with many of its predictions validated, including the precession of Mercury[2], gravitational time dilation and gravitational redshift[3], expansion of the universe[4] and frame-dragging[5]. Given the analogy between the macroscopic Maxwell's equations in complex inhomogeneous media and free-space Maxwell's equations for the background of an arbitrary spacetime metric[6–12], the study of light propagation in artificially engineered optical materials and the motion of massive bodies or light in gravitational fields are closely related. Indeed, the invariance of Maxwell's equations under coordinate transformations has been used to design invisibility cloaks at microwave and optical frequencies[13–19], as well as a vast range of transformation optical devices[20–23]. The analogy has also been proposed to mimic well-known phenomena related to general relativity that are difficult to observe directly using existing astronomical tools. In particular, the transformation optics approach can be used to mimic black holes[24–28], Minkowski spacetimes[29], electromagnetic wormholes[30], cosmic strings[31], the 'Big Bang' and cosmological inflation[32,33], as well as Hawking radiation[34,35]. Although the theoretical foundations behind the design of 'toy' models of general relativity are now well understood, experimental validation of the transformation optics approach to mimicking the scattering of electromagnetic radiation in close proximity to actual celestial objects remains a challenge, especially for visible light.

In this Article, we propose a flexible experimental methodology that allows the direct optical investigation of light trapping around a microsphere (which simulates gravitational lensing due to power-law mass-density/pressure distributions), including light trapping at the photon sphere that is similar to that around compact neutron stars and black holes (Fig. 1a). Our approach uses a microsphere embedded into a planar polymer waveguide (Fig. 1b) formed during a controlled spin-coating process. Because of surface tension effects, the waveguide around the microsphere is distorted, resulting in a continuous change in the waveguide effective refractive index that, under certain conditions, can mimic the curved spacetimes caused by strong gravitational fields. Using direct fluorescence imaging, we observe lensing and asymptotic capture of the incident light in an unstable circular orbit that corresponds to the photon sphere of a compact stellar object. These observations clearly demonstrate that the proposed experimental methodology provides a useful 'toy' model with which to study both near- and far-field electromagnetic effects, under a controlled laboratory environment, that are similar to the gravitational lensing described in general relativity. The experimental observations are in excellent agreement with the developed theory, validating both the derived exact solution of the Einstein field equations and the predicted geodesic trajectories of massless particles in the inherent curved spacetime.

Sample fabrication and optical characterization

A structured waveguide was fabricated for the experiment, as shown in Fig. 1b. A 50-nm-thick silver film was initially deposited on a silica (SiO_2) substrate. A grating with a period of 310 nm was then drilled across the silver film using a focused ion beam (FEI Strata FIB 201, 30 keV, 11 pA). A polymethylmethacrylate (PMMA) resist was mixed with oil-soluble CdSe/ZnS quantum dots (at a volume ratio of 2:1). A powder consisting of microspheres 32 μm in diameter was then added to the mixture. The CdSe/ZnS quantum dots are added for the purpose of fluorescence imaging, while the microspheres provide the important functionality of creating a gradual change in the PMMA thickness (in close proximity to the microspheres), which results in a gradient-index waveguide. The mixture was deposited on the silver film using a spin-coating process, and the sample was dried in an oven at 70 °C for 2 h. During this process, the thickness of the PMMA layer can be controlled by varying the spin rate, evaporation rate and solubility of the PMMA solution. In the zone located far from the microsphere, the PMMA layer is uniformly thick (∼1.0 μm). In the region near the microsphere, the waveguide thickness gradually increases due to surface tension effects before and during the baking process. This phenomenon is indirectly observed by examining the interference pattern (Fresnel zones) around the microsphere (Fig. 2a; the sample is illuminated with white and blue light in the top and bottom panels, respectively). The interference minima and maxima depend on the PMMA thickness and can be used to

[1]National Laboratory of Solid State Microstructures & Department of Physics, National Center of Microstructures and Quantum Manipulation, Nanjing University, Nanjing 210093, China, [2]College of Engineering and Science, Louisiana Tech University, Ruston, Louisiana 71270, USA. *e-mail: liuhui@nju.edu.cn

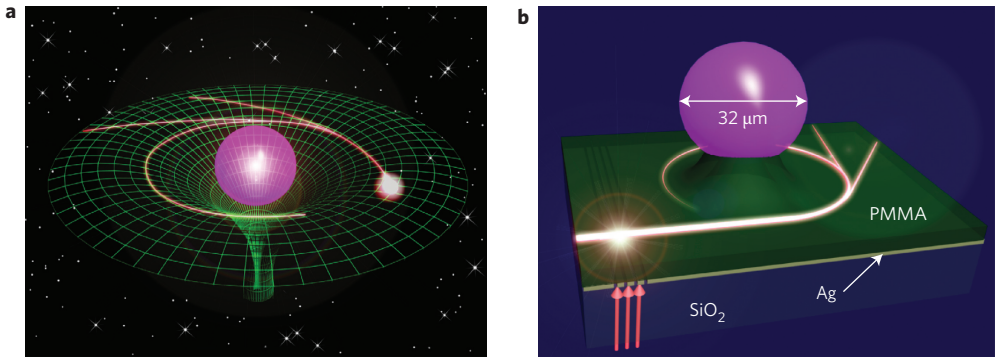

Figure 1 | Analogue of light deflection in a gravitational field and microstructured optical waveguide. a, Depiction of light deflection by the gravitational field of a massive stellar object. **b**, Schematic view of the microstructured optical waveguide formed around a microsphere and used to emulate the deflection of light by a gravitational field. In the experimental set-up, a grating is drilled across a 50-nm-thick silver layer, which is then used to couple the incident laser light into the waveguide. Red arrows denote the incident laser beam.

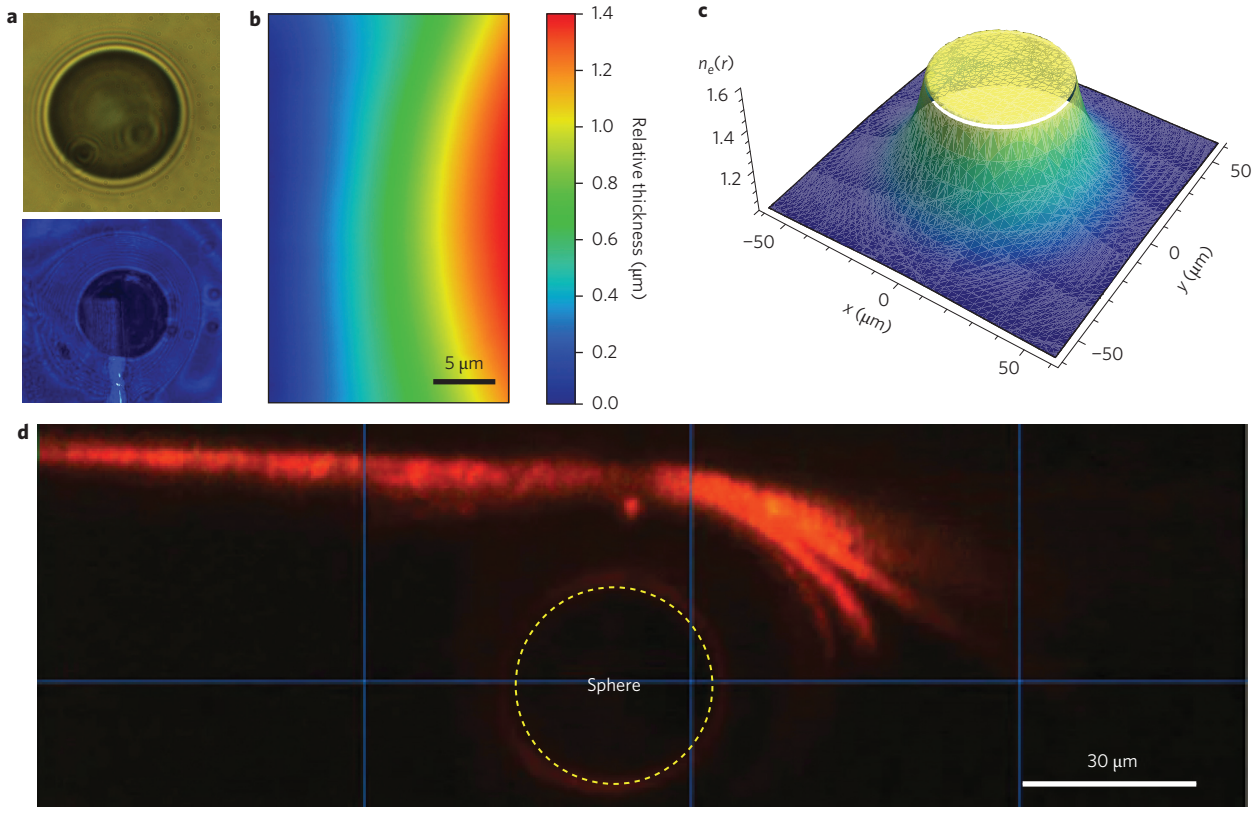

Figure 2 | Structural and optical measurements of the sample. a, Interference pattern around the microsphere illuminated by white (top) and blue (bottom) light. **b**, Surface profile of the PMMA layer measured with AFM. **c**, The effective refractive index of the microstructured waveguide is extracted, showing a strong power-law dependence with radial distance from the microsphere. **d**, A particular example of light bending in close proximity to the microsphere. The incident beam is coupled into the waveguide using a diffraction grating drilled into the metal layer.

extract the thickness profile as a function of the distance to the centre of the microsphere. The surface profile of the PMMA layer can be directly measured using atomic force microscopy (AFM). The measured thickness profile (Fig. 2b) is in good agreement with the results retrieved from the interference measurements.

The light deflection provided by the variable-thickness waveguide and observed in the vicinity of the microsphere can be described using the waveguide effective refractive index. In the experiment, the structured waveguide consists of an air/PMMA/silver/SiO_2 multilayer stack (Fig. 1b) and can be considered as a step-index planar waveguide. The dispersion relationship of the waveguide transverse magnetic (TM) modes (Supplementary Section S1) is used to extract the effective refractive index around the microsphere, which is depicted in Fig. 2c. The waveguide index (for the $TM_{0,6}$ mode) rapidly decreases with distance from the microsphere according to a power-law dependence $n_e^2 \approx n_{e,\infty}^2[1+(a/r)^4]$, where the parameters $a = 28.5$ μm and $n_{e,\infty}^2 = 1.1$ correspond to the best fit. Within the immediate proximity of the microsphere, the refractive index approaches the bulk values for PMMA, $n_{\mathrm{PMMA}}^2 = 2.31$.

To study the ray propagation in close proximity to the microsphere, 405 nm light from a continuous-wave (c.w.) laser was

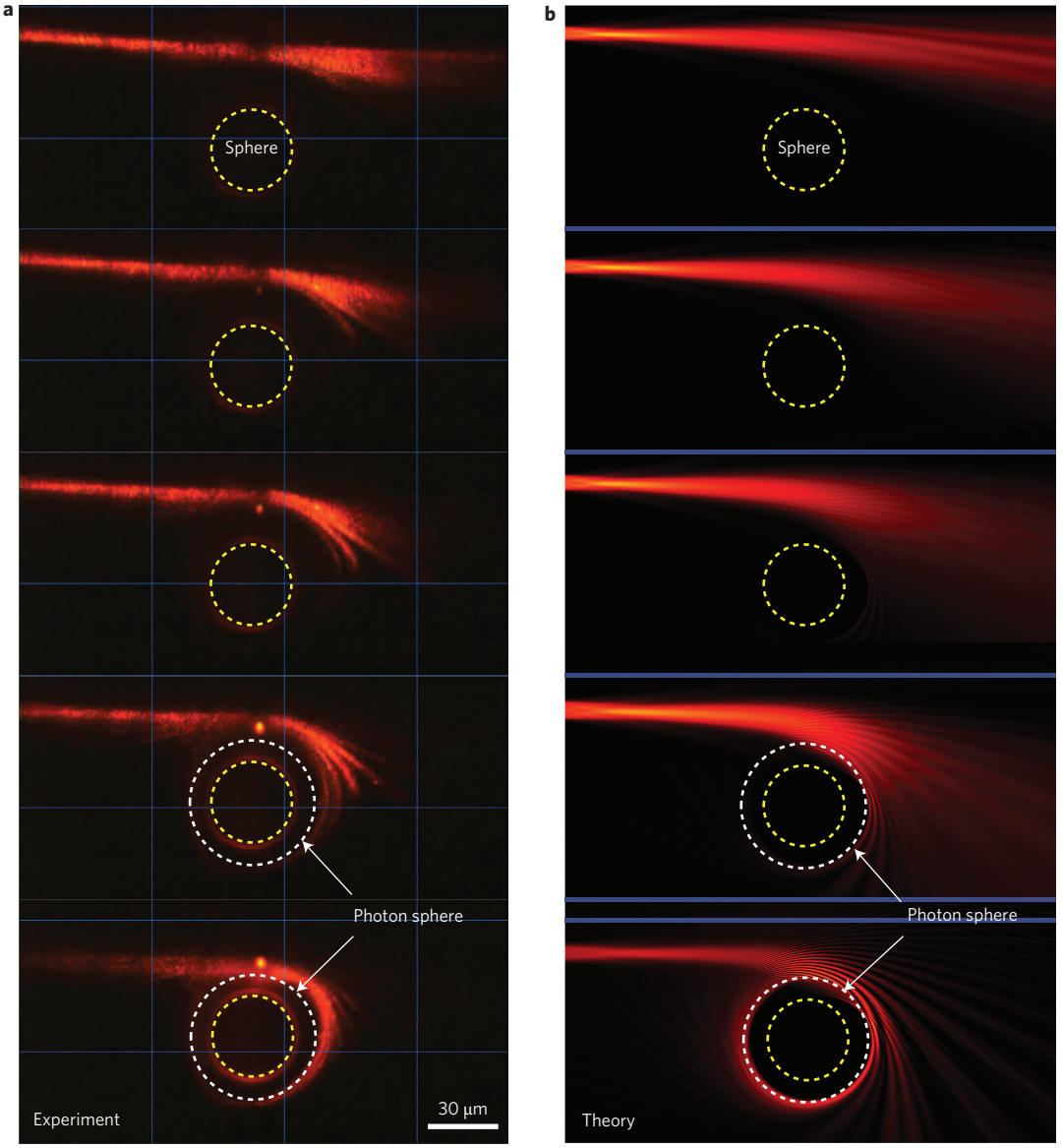

Figure 3 | Scattered field intensity around the microsphere. a,**b**, Scattered field intensity observed in the experiment (**a**) and calculated using a full-wave finite-difference frequency-domain (FDFD) electromagnetic code (**b**). In the calculations, the effective refractive index is extracted from the experimental data. From top to bottom, the incident beam impact parameter is gradually decreased, resulting in a strong increase in beam deflection from the original path. At critical impact parameters (bottom two images), the light rays approach the photon sphere with a fraction of the incident energy scattered away from the microsphere, while the rest is captured around the microsphere.

coupled into the waveguide through a grating (Fig. 1b). As the coupled light propagates within the waveguide, it excites the quantum dots, which then re-emit at 605 nm. The fluorescence emission from the quantum dots was collected by a microscope objective (Zeiss Epiplan ×50/0.17 HD microscope objective) and delivered to a charge-coupled device camera. The obtained fluorescence image was then used to analyse the ray trajectory. One particular example is given in Fig. 2d. The incident light is deflected as it passes within the vicinity of the microsphere. In the following section, this phenomenon is revealed to be closely related to the deflection of light in a centrally symmetric curved spacetime corresponding to degenerated fluid in hydrostatic equilibrium with an asymptotically polytropic equation of state.

The complete range of optical phenomena associated with the proposed microstructured waveguide was mapped by a set of measurements in which the excitation point was gradually moved along the grating and towards the microsphere. See Supplementary Movie for the tuning process used in the experiment, and a demonstration of the gradual increase in light deflection with a decrease in distance to the microsphere. The change in the fluorescence pattern, which captures the interaction of the incident beam with the inhomogeneous effective refractive index of the waveguide, is presented in Fig. 3a. We observe a gradual increase in light deflection as the distance to the microsphere decreases. Owing to the finite excitation spot size, which corresponds to a Gaussian beam waist size ($\sigma \approx 3$ μm), the beam fans out with the outside beam envelope deflected at lower angles. For excitation with an impact parameter (the perpendicular distance between the beam and the centre of the microsphere) approaching the critical value $b_c \approx 39$ μm, the impinging light approaches an unstable photon orbit (that is, a photon sphere) at a radius of $r \approx a$. The photon sphere splits the entire space into two domains such that if the impact parameter is larger than its critical value, the impinging light approaches the microsphere until it reaches a point of closest

approach (turning point) and is then deflected back into space, whereas for impact parameters smaller than critical, the light is captured. To validate our experimental finding, full-wave finite-difference calculations were performed using finite-difference COMSOL Multiphysics software. The theoretically obtained scattering profiles (Fig. 3b) are nearly identical to the experimental data. The two main experimental findings are again observed: (1) the deflection angle increases with decreasing impact parameter and (2) the impinging light is captured by the system for impact parameters below the critical value, $b \leq b_c$. These results are reminiscent of gravitational lensing, as well as the existence of a photon sphere around stellar objects such as ultracompact neutron stars and black holes[36]. Hence, our system may constitute a useful 'toy' model to study electromagnetic scattering and light capture due to such unique astrophysical objects.

Curved spacetimes around the microsphere

To validate the above proposition, we considered static centrally symmetric spacetimes described by the isotropic metric $ds^2 = -g_{00}(r)dt^2 + g_{rr}(r)dx^2$. The metric must be a solution of the Einstein field equations $G_{uv} = -T_{uv}$, with a stress-energy tensor $T_{uv} = \rho u_u u_v + p(u_u u_v - g_{uv})$ that depends on centrally symmetric mass-density ρ and pressure p distributions. The field equations can be solved either by providing the equation of state $p = p(\rho)$, or by using a generating function[36,37]. Here, we rely on the latter approach by enforcing the matching condition (that is, the effective refractive index of the metric $n = \sqrt{g_{rr}/g_{00}}$ (ref. 25) must coincide with that of the experiment), and then proceed to obtain the unknown metric elements, mass density and pressure. The field equations are found to have an exact solution with the metric

$$ds^2 = \frac{A}{r^4 n^4(r)} \csc^2\left(\sqrt{\frac{5}{2}}\cot^{-1}(r^2)\right)\left[-dt^2 + n^2(r)dx^2\right] \qquad (1)$$

where A is an integration constant (Supplementary Section S2). This metric is finite and corresponds to asymptotically flat free space at large distances. The required pressure and mass-density are also obtained, showing an asymptotic (for $r > a$) equation of state $p = k\rho^{1+1/n}$ with a polytropic index $n = 3/2$. A large variety of gravitational objects in hydrostatic equilibrium can satisfy such an equation of state, including degenerate star cores such as those in neutron stars, red giants and white dwarfs, and non-isothermal gas clouds with an interior that is cooler than the exterior[36].

The motion of a light ray in the curved spacetime of equation (1) is described by the Lagrangian $\mathcal{L} = (1/2)(ds/d\tau)^2$ where τ is the trajectory parameter. The Euler–Lagrange equations are then solved, giving an explicit solution for the ray trajectories as a function of the azimuthal angle φ in the form

$$u(\varphi) = u_0 + u_t sn\left(\frac{q(\varphi - \varphi_0)}{u_t}\middle| u_t^4\right) \qquad (2)$$

where $u = a/r$ is the inverse radial coordinate, φ_0 is the angle of incidence, u_0 is the initial position, and sn is the Jacobi elliptic function. The solution depends on the external turning point

$$u_t = a/r_t = (b/b_c)\left(1 - \sqrt{1 - (b_c/b)^4}\right)^{1/2}$$

that is, the position of closest approach. Clearly, for in-falling rays a turning point exists only if the impact parameter is larger than the critical value $b \geq b_c = a\sqrt{2}$, otherwise the rays will be captured within the spatial domain below the photon sphere $r \leq a$. Thus, our system can be described with a total capture cross-length of $\sigma_c = 2b_c = 2a\sqrt{2}$, indicating that any light ray that approaches the microsphere within such a spatial range will be captured. The capture cross-length is independent of the direction from which the light has been emitted, which exemplifies the omnidirectional properties of the system and points towards possible applications in light steering and energy harvesting devices. Finally, the total defection angle for in-falling rays with $b \geq b_c$ is obtained from equation (2) as

$$\theta = 2K\left[u_t^4\right]\sqrt{1 + u_t^4} - \pi \qquad (3)$$

where K is the complete elliptical integral of the first kind. If the incident ray traverses the spatial domain away from the photon sphere ($b \gg b_c$), then $\theta \to 3\pi(b_c/2b)^4$, and an inverse power-law dependence of the deflection angle with the impact parameter is observed. This indicates that objects described with metric equation (1) will exhibit gravitational lensing with an equivalent lens equation of the form, $1/s_1 + 1/s_2 = 1/f$, where the 'focal' length $f = 4a/3\pi u_t^5$ depends on the distance of the closest approach $r_t = a/u_t$, commonly referred to as the Einstein ring radius, and s_1 and s_2 are the distances to the source and image, respectively.

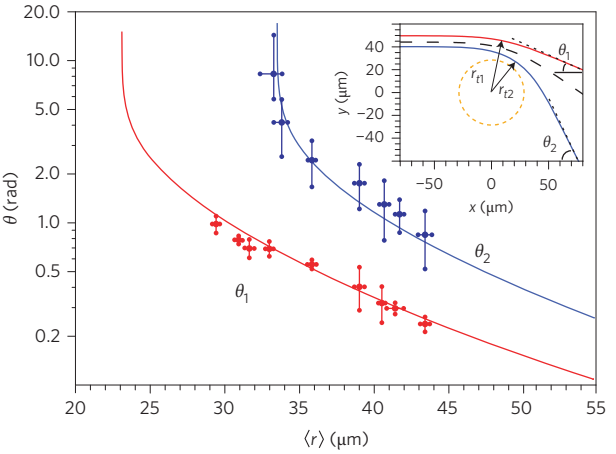

Figure 4 | Deflection angles. Deflection angles measured in the experiment (symbols) and calculated (red and blue lines) based on equation (3). Because of the final width of the incident light beam, two deflection angles θ_1 and θ_2, corresponding to the edges of the beam (at 1/e intensity), can be extracted unambiguously. The beam envelope is then represented by two points of closest approach r_{t1} and r_{t2}, corresponding to the two deflection angles shown in the inset and calculated using equation (2). For the purpose of presentation we depict the deflection angles as a function of the geometrical average between the two turning distances: $\langle r \rangle = (r_{t1} + r_{t2})/2$. Error bars due to the experiment are also included. The experimental data closely match the theory for all measured cases. A singularity in the deflection angle is observed for $r_{t2} \approx a = 28.5$ μm, corresponding to the photon sphere of our system.

A comparison between the experimentally measured and theoretically obtained deflection angles is shown in Fig. 4. Given that the incident beam in the experiment has a finite size, two deflection angles can be unambiguously extracted from the experiment, particularly those that correspond to the beam envelope impact parameters $b_\pm = b_0 \pm \sigma$, where b_0 is the impact parameter that corresponds to the maximum beam intensity. The deflection angles are then plotted versus the geometric average of the two distances of closest approach (Fig. 4, inset). The experimental data are consistent with the theoretical findings, indicating that our experimental method can describe both the far-field scattering and the critical behaviour close to the photon sphere corresponding to the curved spacetimes given by equation (1). Aside from light deflection, the gravitational time delay (or Shapiro effect) may also be

investigated using our experimental set-up. We must note that within extended stellar objects, other than gravitational effects, light rays will also be affected by the object material constituents (charged particles, atoms and molecules). These types of scattering processes, while important, are rather complex in nature and go beyond the scope this work, which only aims to investigate the effects of gravity.

In conclusion, we have experimentally demonstrated an optical analogue of the effects of gravity on the motion of light rays, including light deflection, Einstein rings and photon capture. The 'gravitational field' effect is achieved using an inhomogeneous effective refractive index provided by a microstructured waveguide spin-coated in the presence of a microsphere. The deflection and capture of light are directly observed based on the fluorescence imaging method. An exact solution of the Einstein field equations is obtained showing that the proposed 'toy' model can mimic the effect of gravity due to a spherically symmetric object in hydrostatic equilibrium with an asymptotically polytropic equation of state. Our method may also be applied to control light propagation in integrated optoelectronic elements, light splitters and benders, omnidirectional absorbers and energy harvesting devices.

Received 1 January 2013; accepted 21 August 2013; published online 29 September 2013

References

1. Dyson, F. W., Eddington, A. S. & Davidson, C. A determination of the deflection of light by the Sun's gravitational field, from observations made at the total eclipse of May 29, 1919. *Phil. Trans. R. Soc. Lond. A* **220,** 291–333 (1920).
2. Kramer, M. *et al.* Tests of general relativity from timing the double pulsar. *Science* **314,** 97–102 (2006).
3. Hafele, J. C. & Keating, R. E. Around-the-world atomic clocks: predicted relativistic time gains. *Science* **177,** 166–168 (1972).
4. Bennett, C. L. Cosmology from start to finish. *Nature* **440,** 1126–1131 (2006).
5. Everitt, C. W. F. *et al.* Gravity probe B: final results of a space experiment to test general relativity. *Phys. Rev. Lett.* **106,** 221101 (2011).
6. Pendry, J. B., Schurig, D. & Smith, D. R. Controlling electromagnetic fields. *Science* **312,** 1780–1782 (2006).
7. Leonhardt, U. Optical conformal mapping. *Science* **312,** 1777–1780 (2006).
8. Shalaev, V. M. Transforming light. *Science* **322,** 384–386 (2008).
9. Li, J. & Pendry, J. B. Hiding under the carpet: a new strategy for cloaking. *Phys. Rev. Lett.* **101,** 203901 (2008).
10. Lai, Y. *et al.* Illusion optics: the optical transformation of an object into another object. *Phys. Rev. Lett.* **102,** 253902 (2009).
11. Chen, H., Chan, C. T. & Sheng, P. Transformation optics and metamaterials. *Nature Mater.* **9,** 387–396 (2010).
12. Leonhardt, U. & Philbin, T. G. General relativity in electrical engineering. *New J. Phys.* **8,** 247 (2006).
13. Schurig, D. *et al.* Metamaterial electromagnetic cloak at microwave frequencies. *Science* **314,** 977–980 (2006).
14. Cai, W., Chettiar, U. K., Kildishev, A. V. & Shalaev, V. M. Optical cloaking with metamaterials. *Nature Photon.* **1,** 224–227 (2007).
15. Alù, A. & Engheta, N. Multifrequency optical invisibility cloak with layered plasmonic shells. *Phys. Rev. Lett.* **100,** 113901 (2008).
16. Valentine, J. *et al.* An optical cloak made of dielectrics. *Nature Mater.* **8,** 568–571 (2009).
17. Gabrielli, L. H., Cardenas, J., Poitras, C. B. & Lipson, M. Silicon nanostructure cloak operating at optical frequencies. *Nature Photon.* **3,** 461–463 (2009).
18. Smolyaninov, I. I., Smolyaninova, V. N., Kildishev, A. V. & Shalaev, V. M. Anisotropic metamaterials emulated by tapered waveguides: application to optical cloaking. *Phys. Rev. Lett.* **102,** 213901 (2009).
19. Ergin, T. *et al.* Three-dimensional invisibility cloak at optical wavelengths. *Science* **328,** 337–339 (2010).
20. Rahm, M., Roberts, D. A., Pendry, J. B. & Smith, D. R. Transformation-optical design of adaptive beam bends and beam expanders. *Opt. Express* **16,** 11555–11567 (2008).
21. Ma, Y. G., Ong, C. K., Tyc, T. & Leonhardt, U. An omnidirectional retroreflector based on the transmutation of dielectric singularities. *Nature Mater.* **8,** 639–642 (2009).
22. Cheng, Q., Cui, T. J., Jiang, W. X. & Cai, B. G. An omnidirectional electromagnetic absorber made of metamaterials. *New J. Phys.* **12,** 063006 (2010).
23. Zentgraf, T. *et al.* Plasmonic Luneburg and Eaton lenses. *Nature Nanotech.* **6,** 151–155 (2011).
24. Leonhardt, U. & Piwnicki, P. Optics of nonuniformly moving media. *Phys. Rev. A* **60,** 4301–4312 (1999).
25. Genov, D. A., Zhang, S. & Zhang, X. Mimicking celestial mechanics in metamaterials. *Nature Phys.* **5,** 687–692 (2009).
26. Narimanov, E. E. & Kildishev, A. V. Optical black hole: broadband omnidirectional light absorber. *Appl. Phys. Lett.* **95,** 041106 (2009).
27. Chen, H., Miao, R.-X. & Li, M. Transformation optics that mimics the system outside a Schwarzschild black hole. *Opt. Express* **18,** 15183–15188 (2010).
28. Genov, D. A. Optical black-hole analogues. *Nature Photon.* **5,** 76–78 (2011).
29. Smolyaninov, I. I. & Narimanov, E. E. Metric signature transitions in optical metamaterials. *Phys. Rev. Lett.* **105,** 067402 (2010).
30. Greenleaf, A., Kurylev, Y., Lassas, M. & Uhlmann, G. Electromagnetic wormholes and virtual magnetic monopoles from metamaterials. *Phys. Rev. Lett.* **99,** 183901 (2007).
31. Mackay, T. G. & Lakhtakia, A. Towards a metamaterial simulation of a spinning cosmic string. *Phys. Lett. A* **374,** 2305–2308 (2010).
32. Smolyaninov, I. I. & Hung, Y.-J. Modeling of time with metamaterials. *J. Opt. Soc. Am. B* **28,** 1591–1595 (2011).
33. Ginis, V., Tassin, P., Craps, B. & Veretennicoff, I. Frequency converter implementing an optical analogue of the cosmological redshift. *Opt. Express* **18,** 5350–5355 (2010).
34. Philbin, T. G. *et al.* Fiber-optical analog of the event horizon. *Science* **319,** 1367–1370 (2008).
35. Belgiorno, F. *et al.* Hawking radiation from ultrashort laser pulse filaments. *Phys. Rev. Lett.* **105,** 203901 (2010).
36. Misner, C. W., Thorne, K. S. & Wheeler, J. A. *Gravitation* (W. H. Freeman, 1973).
37. De Felice, F. On the gravitational field acting as an optical medium. *Gen. Relativ. Gravit.* **2,** 347–357 (1971).

Acknowledgements

This work was supported by the National Key Projects for Basic Researches of China (nos 2012CB933501, 2010CB630703 and 2012CB921500), the National Natural Science Foundation of China (nos 11074119, 60990320 and 11021403), the Louisiana Board of Regents and National Science Foundation (contract nos LEQSF (2007-12)-ENH-PKSFI-PRS-01, LEQSF (2011-14)-RD-A-18), the Project Funded by the Priority Academic Program development of Jiangsu Higher Education Institutions (PAPD), New Century Excellent Talents in University (NCET-10-0480), a doctoral program (20120091140005) and Dengfeng Project B of Nanjing University.

Author contributions

C.S., H.L., Y.W. and S.N.Z. proposed and carried out the experiment. D.A.G. contributed to the experimental characterization and interpretation, and proposed and developed the theory. D.A.G., C.S. and H.L. co-wrote the manuscript.

Additional information

Supplementary information is available in the online version of the paper. Reprints and permissions information is available online at www.nature.com/reprints. Correspondence and requests for materials should be addressed to H.L.

Competing financial interests

The authors declare no competing financial interests.

nature photonics

SUPPLEMENTARY INFORMATION

DOI: 10.1038/NPHOTON.2013.247

Trapping light by mimicking gravitational lensing

C. Sheng[1], H. Liu[1], Y. Wang[1], S. N. Zhu[1], and D. A. Genov[2]

[1]National Laboratory of Solid State Microstructures & Department of Physics, Nanjing University, Nanjing 210093, People's Republic of China

[2]College of Engineering and Science, Louisiana Tech University, Ruston, Louisiana 71270, USA

I. Experimental measurements, fittings and effective permittivity

The poly-methyl-methacrylate (PMMA) thickness profiles were measured using two different methods: (a) direct Atomic Force Microscopy (AFM), and (b) interference data. The results are shown in Figure 1. The measured film thickness at large distances is then fitted with a power law function of the type

$$h(r) \approx h_\infty \left(1 + \left(\frac{R}{r}\right)^s\right) \qquad (1)$$

where h_∞ is the film thickness at infinity. The experimental data are presented in Figure 1 while the fitting parameters are listed in Table 1. Both the AFM data and interference data show almost the same far-distance behaviors with similar power law exponents of about $s = 4$. The effective refractive waveguide index (permittivity) is obtained by considering the structured waveguide geometry consisting of Air/PMMA/Silver/SiO_2 multilayer stack. For transverse magnetic (TM) waves, the dispersion relationship is given as:

$$\exp[2ik_2h] = \frac{1 + r_{32}r_{43}\exp[2ik_3t]}{r_{12}r_{32} + r_{12}r_{43}\exp[2ik_3t]} \qquad (2)$$

where $r_{ik} = (\eta_k - \eta_i)/(\eta_k + \eta_i)$ are the reflection coefficients, t is the metal layer thickness, the specific impedances and transversal wave vectors are $\eta_i = \left(n_i^2 - n_e^2\right)^{1/2}/n_i^2$ and $k_i = (\omega/c)\left(n_i^2 - n_e^2\right)^{1/2}$, respectively, where n_e is the effective waveguide index and n_i are the refractive indexes of each media ((1)-air, (2)-PMMA, (3)-Silver, and (4)-Glass). Note that Eq. (2) cannot be solved explicitly with respect to the effective index but it can be solved with respect to the film thickness giving

$$h = \frac{1}{k_2}\left(m\pi + \frac{1}{2i}\ln\left(\frac{1 + r_{32}r_{43}\exp[2ik_3t]}{r_{12}r_{32} + r_{12}r_{43}\exp[2ik_3t]}\right)\right) \qquad (3)$$

where m is the mode index. For sufficiently thick metal layers Eq. (3) can be significantly simplified as

$$h = \frac{1}{k_2}\left(m\pi + \frac{i}{2}\ln(r_{12}r_{32})\right) \qquad (4)$$

DOI: 10.1038/NPHOTON.2013.247

The dispersion relationship for the first seven modes calculated using Eq. (3) and Eq. (4) are shown in Figure 1c. In the calculations we use: $n_{SiO_2} = 1.47$[1], $n_{PMMA} = 1.51$[2], and at the operation wavelength $\lambda = 405nm$, the silver index $n_{Ag} = 0.05 + i2.275$ is taken from Johnson&Christy[3]. The metal film thickness is set at $t = 50nm$. Clearly, the metal layer is sufficient thick to reduce the problem into a single dielectric waveguide on a top of a semi-infinite metal substrate. The estimated effective refractive index (permittivity) is then fitted to a power law function of the type

$$\varepsilon(r) = n^2(r) \approx n_\infty^2 \left[1 + \left(\frac{a}{r}\right)^4\right] \qquad (5)$$

where n_∞ is the effective refractive index at infinity, and a is the photon sphere radius (see below). The fitting parameters are included in Table 1.

Data type	$h_\infty[\mu m]$	$R[\mu m]$	s	$a[\mu m]$
AFM	1.0515	26.542	4.042	28.5
Interference	1.071	26.43	4.245	27.96

Table 1. Experimental fitting parameters for the polymethylmethacrylate (PMMA) film thickness and effective refractive index of the $TM_{0,6}$ mode.

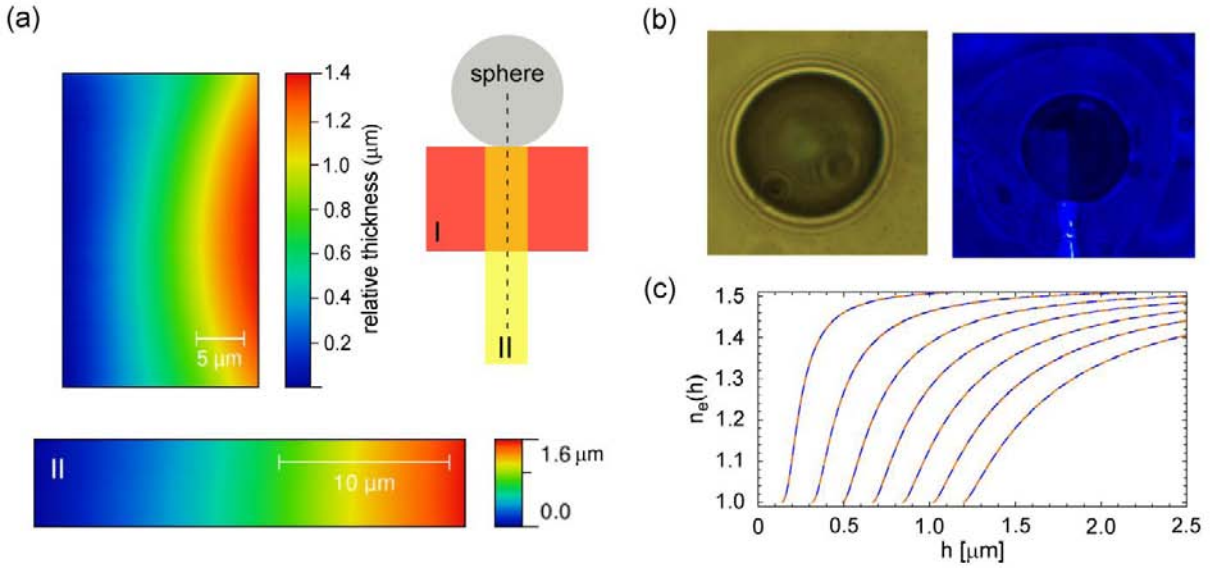

Figure 1. Film thickness measured using (a) atomic force microscope (AFM) data and (b) interference data. (c) The effective refraction index is calculated using Eq. (3) (blue solid line) and Eq. (4) (orange dashed line).

II. Centrally-symmetric isotropic spacetimes

Einstein field equations: Here, we seek to identify a curved spacetime that can provide optical effects similar to those observed in the experiment. We begin by considering a static centrally symmetric spacetime in homogeneous coordinates

$$ds^2 = e^{2\nu}c^2dt^2 - e^{2\lambda}\left(dr^2 + r^2d\Omega^2\right) \qquad (6)$$

where the metric functions ν and λ depend on the radial coordinate only. The metric elements are solution of the Einstein field equations

$$G_{\mu\nu} = -T_{\mu\nu} = -\rho u_\mu u_\nu - p\left(u_\mu u_\nu - g_{\mu\nu}\right)$$

where u_μ are the 4-velocities and we have adopted a system of units with $8\pi G = c = 1$. Following a standard procedure[4] the governing equations are as follows:

$$\begin{gathered}\rho = -\frac{e^{-2\lambda}}{r}\left(2r\lambda'' + \lambda'(4 + r\lambda')\right) \\ p = \frac{e^{-2\lambda}}{r}\left(2\nu'(1 + r\lambda') + \lambda'(2 + r\lambda')\right) \\ (\rho + p)\nu' + p' = 0\end{gathered} \qquad (7)$$

The above equations are solved either by providing the equation of state $p = p(\rho)$, or by using a generating function. Here we will rely on the later by introducing the effective refractive index of the metric

$$n^2 = e^{2(\lambda-\nu)}, \quad \lambda(r) = \nu(r) + \ln[n(r)]\,.$$

Working with the non-dimensional radial coordinate $\frac{r}{a} \to r$ we obtain an analytical solution of Eq.7 with the metric elements given as

$$e^{2\lambda} = -\frac{A}{1 + r^4}\sec^2(\varphi + \delta), \quad e^{2\nu} = -\frac{Ar^4}{(1 + r^4)^2}\sec^2(\varphi + \delta) \qquad (8)$$

where $\varphi = \sqrt{5/2}\cot^{-1}(r^2)$, $\delta \in \mathbb{R}$ and $A \in \mathbb{R}$ are the integration constants. All unique solutions are obtained for $\delta \in \left(-\frac{\pi}{2}, \frac{\pi}{2}\right)$.

Mass-density and pressure: The mass-density and pressures are obtained from Eqs. 7 and 8

$$\rho = \frac{6\sin[\varphi + \delta]\left(5r^2\sin[\varphi + \delta] + \sqrt{10}(r^4 - 1)\cos[\varphi + \delta]\right)}{A(1 + r^4)}$$

$$p = -\frac{2 + 9r^4 + 2r^8 + (2 - 21r^4 + 2r^8)\cos[2(\varphi + \delta)] + 4\sqrt{10}r^2(r^4 - 1)\sin[2(\varphi + \delta)]}{Ar^2(1 + r^4)}$$

DOI: 10.1038/NPHOTON.2013.247

Special case - finite pressure and mass density at large distances: The only solution with finite positive pressure and density at large distances is obtained for $\delta = \pm\frac{\pi}{2}$, with the metric given as

$$ds^2 = A\left(\frac{\csc(\varphi)}{r^2 n^2(r)}\right)^2 [-dt^2 + n^2(r)d\vec{x}^2] \qquad (9)$$

where $A > 0$.The metrics is finite and asymptotically flat at large distances(see Fig. 2).

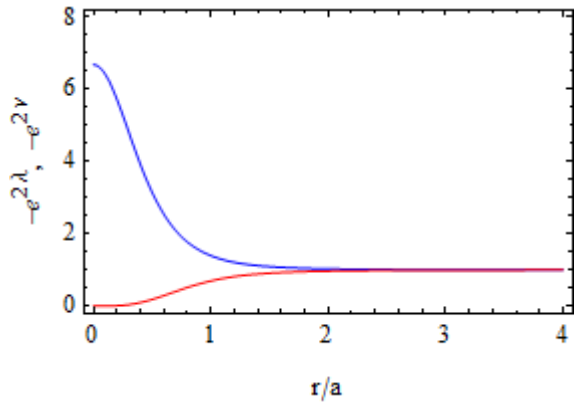

Figure 2 The metric elements for $\delta = \pm\frac{\pi}{2}$and $A = 5/2$.

The pressure and mass-density are

$$\rho = 3\frac{5r^2 + 5r^2\cos[2\varphi] + \sqrt{10}(1-r^4)\sin[2\varphi]}{A(1+r^4)}$$
$$p = \frac{(2 - 21r^4 + 2r^8)\cos[2\varphi] - 4\sqrt{10}r^2(1-r^4)\sin[2\varphi] - 2 - 9r^4 - 2r^8}{Ar^2(1+r^4)}$$

Both, the pressure and the mass density are positive for $r \geq r_c = a\sqrt{\cot(\pi/\sqrt{10})} = 0.8071a$ which is the range where the effective refractive index fit (Eq. 5) is valid. Clearly, any physically meaningful solution that covers the entire space must be formed by switching the metrics Eq. 9 with some other interior solution that is valid for $r < a$. At large distances we have

$$\rho = \frac{15}{A}r^{-6} + O(r^{-10}), \quad p = \frac{3}{2A}r^{-10} + O(r^{-14})$$

which corresponds to an equation of state $p = k\rho^{5/3} = k\rho^{1+1/n}$, or a polytrop with n = 3/2. Such equation of state is typical for degenerate star cores including degenerated neutron stars, red giants, white and brown dwarfs.

Geodesic trajectories: Here, we consider the trajectories of massive/massless particles in the spacetime described by the metrics Eq. 9 which we now recast as

$$ds^2 = g_{00}(r)\left[-dt^2 + n^2(r)\left(dr^2 + r^2 d\Omega^2\right)\right] \qquad (10)$$

The Lagrangian $\mathcal{L}$ and the Euler-Lagrange equations for a ray motion restricted to the $\theta = \pi/2$ plane follows

$$\begin{aligned} \mathcal{L} = \kappa = \frac{1}{2}\left(\frac{ds}{d\tau}\right)^2 = \frac{1}{2} g_{00}(r)[-\dot{t}^2 + n^2(r)(\dot{r}^2 + r^2\dot{\varphi}^2)] \\ \dot{\varphi} = \frac{d\varphi}{d\tau} = \frac{a}{g_{00}(r)n^2(r)r^2}, \quad \dot{t} = \frac{dt}{d\tau} = \frac{a}{b g_{00}(r)} \end{aligned} \qquad (11)$$

where a and b are constants of motion related to the total energy and angular momentum of the particle, τ is an affine parameter and $\kappa = 1/0$ for massive/massless particle.Using the azimuthal angle φ as the parameter of the trajectory, the equation of motion (first integral) for a massless particle is obtained from Eq. 11

$$\left(\frac{dr}{d\varphi}\right)^2 = \frac{n^2(r)r^4}{b^2} - r^2 \qquad (12)$$

Deflection angle: Here, we seek to obtain an analytical solution of Eq. 12 with the use of the experimentally measured effective refractive index Eq. 5. It is convenient to use the inverse radial coordinate $u = a/r$, and Eq. (12) now reads

$$\left(\frac{du}{d\varphi}\right)^2 = q^2(1 + u^4) - u^2 \qquad (13)$$

where $q = a/b$ is a constant. This equation has both implicit and explicit solutions in the form

$$\begin{aligned} \varphi(u) = \varphi_0 + (1 + u_t^4)^{1/2} F\left(\sin^{-1}\left(\frac{u}{u_t}\right)\middle| u_t^4\right) \\ u(\varphi) = u_0 + u_t \mathrm{sn}\left(\frac{q(\varphi - \varphi_0)}{u_t}\middle| u_t^4\right) \end{aligned} \qquad (14)$$

where φ_0 is the angle of incidence, u_0 is the initial position, F is the elliptic integral of the first kind, and sn is the Jacobi elliptic function. The solution depends on the external turning point,

$$u_t = \frac{a}{r_t} = \frac{1}{q\sqrt{2}}\left(1 - \sqrt{1 - 4q^4}\right)^{\frac{1}{2}} = (b/b_c)\left(1 - \sqrt{1 - (b_c/b)^4}\right)^{1/2} \qquad (15)$$

From Eq. (15) it follows that a turning point u_t (position of closest approach) exist for in-falling rays only if $q \leq 1/\sqrt{2}$ or the impact parameter is larger than the critical value $b \geq b_c = a\sqrt{2}$. The position of the photon sphere is at $r_{ph} = a$ and the internal turning point is $1/u_t$. The turning points and the complete phase space diagram are shown in Fig. 3. Finally, the deflection angle is obtained from Eq. (14) and Eq. (15) and depends on the turning point or equivalently the impact parameter

DOI: 10.1038/NPHOTON.2013.247

$$\theta = 2K[u_t^4]\sqrt{1+u_t^4} - \pi \qquad (16)$$

where K is the complete elliptical integral of the first kind. If the incident ray is far from the photon sphere ($b \gg b_c$), then $q \ll 1$ and we can simplify Eq. (16) to obtain

$$\theta \to \frac{3\pi q^4}{4} = 3\pi\left(\frac{b_c}{2b}\right)^4 \qquad (17)$$

For rays with impact parameters close to the critical ($b \approx b_c$) the deflection angle experiences a logarithmic singularity, which is easily obtained by expanding Eq. (16)

$$\theta \to \frac{1}{\sqrt{2}}\ln\left(\frac{16}{1-b_c/b}\right) - \pi \qquad (18)$$

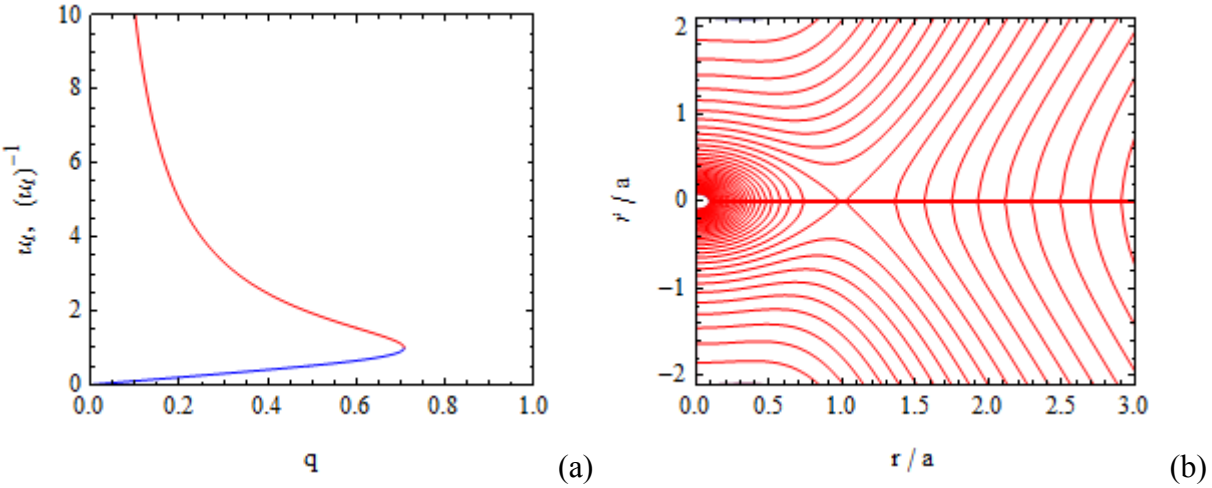

Figure 3(a) The external (blue) and internal (red) turning points, (b) phase space diagram corresponding to the experimentally fitted effective refractive index Eq. 5.

Scattering and capture cross-lengths: Eqs. (15) and (16), can be used to obtain the scattering differential cross-length

$$\frac{d\sigma(\theta)}{d\theta} = \left|\frac{db}{d\theta}\right| = \left|\frac{db}{du_t}\Big/\frac{d\theta}{du_t}\right| = \frac{a}{4u_t}\left|\frac{(1-u_t^4)^2}{(1+u_t^4)E[u_t^4]-(1-u_t^4)K[u_t^4]}\right| \qquad (19)$$

For small angles we have

$$\frac{d\sigma(\theta)}{d\theta} \approx \frac{a(3\pi)^{1/4}}{4\sqrt{2}\theta^{5/4}} \qquad (20)$$

The total capture cross-length is $\sigma_t = 2b_c = 2a\sqrt{2}$, whereas the total scattering cross-length is infinite due to the long range interactions.

Lens equation: The long-distance result Eq. (17) allows writing an equivalent lens equation in the form

$$\frac{1}{s_1}+\frac{1}{s_2}=\frac{1}{f} \qquad (21)$$

where $f = 4a/3\pi u_t^5$ is the equivalent "focal" length which depends on the distance of closest approach $r_t = a/u_t$ or the Einstein ring radius; and s_1 and s_2 are the distances to the center of the source and image, respectively.

III. References

[1]S. N. Kasarova et al. "Analysis of the dispersion of optical plastic materials", Optical Materials **29**, pp. 1481-1490 (2007).
[2] I. H. Malitson,"Interspecimen Comparison of the Refractive Index of Fused Silica", JOSA**55**, Issue 10, pp. 1205-1208 (1965).
[3] P. B. Johnson and R. W. Christy, "Optical Constants of the Noble Metals", Phys. Rev. B **6**, pp. 4370-4379 (1972).
[4]L. D. Landau, E. M. Lifshitz, "The Classical Theory of Fields", Butterworth Heinemann (1995).